Peer-reviewed version available at Gels 2018, 4, 68; doi:10.3390/gels4030068

Article

A methylcellulose hydrogel as support for 3D plotting of complex shaped calcium phosphate scaffolds

Tilman Ahlfeld[1], Tino Köhler[1], Charis Czichy[2], Anja Lode[1]* and Michael Gelinsky[1]*

1 Centre for Translational Bone, Joint and Soft Tissue Research, University Hospital Carl Gustav Carus and Faculty of Medicine, Technische Universität Dresden, Dresden, Germany
2 Institute of Fluid Mechanics, Chair of Magnetofluiddynamics, Measuring and Automation Technology, Technische Universität Dresden, Dresden, Germany
• Correspondence: michael.gelinsky@tu-dresden.de; Tel.: +49-351-4586694, anja.lode@tu-dresden.de; Tel.: +49-351-45816692

Abstract: 3D plotting is an additive manufacturing technology enabling biofabrication, thus the integration of cells or biologically sensitive proteins or growth factors into the manufacturing process. However, most (bio-)inks developed for 3D plotting were not shown to be processed into clinical relevant geometries comprising critical overhangs and cavities, which would collapse without a sufficient support material. Herein, we have developed a support hydrogel ink based on methylcellulose (mc), which is able to act as support as long as the co-plotted main structure is not stable. Therefore, 6 w/v %, 8 w/v % and 10 w/v % mc were allowed to swell in water, resulting in viscous inks, which were characterized for their rheological and extrusion properties. The successful usage of 10 w/v % mc as support ink was proven by multichannel plotting of the support together with a plottable calcium phosphate cement (CPC) acting as main structure. CPC scaffolds displaying critical overhangs or a large central cavity could be plotted accurately with the newly developed mc support ink. The dissolution properties of mc allowed complete removal of the gel without residuals, once CPC setting was finished. Finally, we fabricated a scaphoid bone model by computed tomography data acquisition and co-extrusion of CPC and the mc support hydrogel.

Keywords: calcium phosphate cement, methylcellulose, 3D plotting, support, hydroxyapatite

1. Introduction

In the past, high-temperature extrusion based additive manufacturing, known as fused deposition modeling (FDM) was used to fabricate scaffolds with high diversity of shapes.[1,2] Low-temperature extrusion, called 3D plotting, was shown to combine the geometrical features of FDM with more advanced functionalities like inclusion of proteins and growth factors or bioplotting of cell-laden scaffolds with spatially defined cell distribution.[3,4] However, in contrast to FDM, until now 3D plotting of either cell-laden bioinks or cell-free biomaterial inks rarely was shown for manufacturing complex shaped, volumetric constructs (> 10x10x10 mm^3).[5] These shapes include critical overhangs which produce a bending moment which cannot be balanced by the main body of the scaffold and cavities which collapse due to gravity. Even the fabrication of constructs without flat side (created by deposition of material on the flat building platform of the printer) is impossible. Maybe therefore it is common until now that most publications show the fabrication of an ear-shaped model to demonstrate the capability of novel materials or printing technologies, but an ear displays neither a critical overhang nor a cavity, but has a flat bottom side.

Peer-reviewed version available at Gels 2018, 4, 68; doi:10.3390/gels4030068

Multichannel plotting of a temporary supporting material together with the actual main ink could extend the shape diversity of 3D plotted constructs. An ideal ink should comprise two functionalities: (i) the material ink acts as support for the main ink, preventing plotted strands from collapsing; (ii) the material ink acts as sacrificial material, which means that it is vanishing after post-processing and stabilization of the main scaffold. Additionally, material inks applicable for 3D plotting of support structures must not only meet the requirements mentioned, but also those of viscosity, plottability and post-plotting stability. Within this manuscript, the term *support ink* is used, however the developed biomaterial ink also meets the requirement acting as sacrificial material.

Hydrogels have been developed for several applications of 3D plotting and their viscoelastic properties make them ideal for usage not just as bioink but also as cell-free support ink.[6] Water-soluble methylcellulose (mc) could be a promising candidate. Mc is a synthetic cellulose ether with methyl groups substituting hydrogen atoms of the cellulose molecules. It showed unique viscosity enhancement of aqueous solutions, as well as increased dissolution properties at decreasing temperatures (sol-gel transition was observed in a temperature range between 30-50 °C, depending on the molecular weight).[7,8] Already in the 1940's mc was investigated for medical use in ophthalmology [9] and furthermore is registered in the list of *Inactive Ingredients Search for Approved Drug Products* by the FDA,[10] minimizing the risk of negative effects caused by possible residues at the main scaffold.

For our study, we have chosen to use a ceramic calcium phosphate cement (CPC) as main ink. CPC are composites of inorganic precursors and an aqueous solution. In contact with water molecules, the setting process of CPC is initiated and, for example just like within this work, α-tricalcium phosphate is precipitating to nanocrystalline hydroxyapatite (HAp). Nonetheless, the usage of the classical cements does not allow fabrication by 3D plotting (or sometimes also referred to as robocasting), as the fast setting process leads to needle clogging. Therefore, organic carrier liquids were developed substituting the aqueous phase. They were shown to retard the hydroxyapatite precipitation reaction [11–13] and prevent needle clogging, enabling extrusion of CPC for a sufficient time to fabricate scaffolds. After extrusion to scaffolds and setting of the scaffolds either in water or water-saturated atmosphere, pure nanocrystalline and resorbable HAp scaffolds were achieved demonstrating high potential for bone applications in vivo.[14–16]

Within this paper, we investigated the suitability of mc as support ink for CPC constructs, carried out by multichannel plotting of mc and CPC. We aimed to (i) develop a mc paste fitting the support ink requirements, which was (ii) characterized for its extrusion and plotting properties. Based on these results, CPC constructs were fabricated with (iii) critical overhangs and (iv) cavities in order to enable fabrication of complex shaped CPC constructs, suitable as scaffolds for bone reconstruction or tissue engineering purposes.

2. Results

2.1. Development and rheological characterisation of methylcellulose based support inks

Methylcellulose was dissolved in water in three different concentrations: 6 w/v %, 8 w/v % and 10 w/v %; therefore the resulting support inks within this manuscript are referred to as mc6, mc8 and mc10, respectively. Higher concentrations of mc were excluded of this study, as it was not possible to achieve homogeneous gels with uniform viscosity. Furthermore a low concentration was intended to be advantageous in terms of the sacrificial behaviour of mc inks. It was decided to dissolute mc at 4 °C to ensure full hydration of the mc chains. After complete dissolution, all three combinations, mc6, mc8 and mc10, were almost transparent, homogeneous and viscous pastes, which were used for further characterisation.

Peer-reviewed version available at Gels 2018, 4, 68; doi:10.3390/gels4030068

To evaluate suitability of the pastes for 3D plotting, rheological properties at increasing shear rates were investigated (Figure 1 A). All pastes showed shear thinning behaviour, which is the most important property of inks for extrusion based application. As expected, the viscosity of mc pastes was highly dependent on the concentration; mc10 showed highest viscosity, followed by mc8 and mc6. Exemplarily, the viscosity of the biomaterial inks at a shear rate of 10 s^{-1} was evaluated (Figure 1 B). The viscosity of mc6 was 101.9±6.6 Pas and siginificantly lower compared to mc8 (224.7±7.8 Pas) and mc10 (377.5±16.6 Pas).

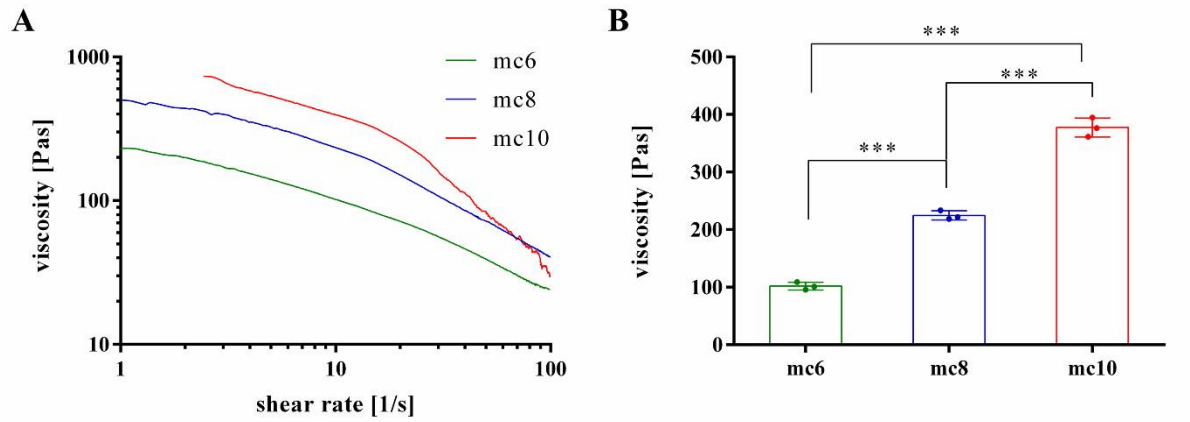

Figure 1. Rheological investigations on shear thinning behavior of mc6, mc8 and mc10 support bioinks. (**A**) Representative viscosity measurements at increasing shear rates; (**B**) Viscosity at a shear rate of 10 s^{-1} (mean ± SD, ***p<0.001, n=3).

Furthermore, the shear recovery of the support inks was tested, following the proposed protocols of Paxton and co-workers and Kesti and co-workers.[17,18] Therefore, firstly a low shear rate of 5 s^{-1} was applied for 200 s, followed by a hundred-fold higher shear rate of 500 s^{-1} for 100 s. This procedure was repeated two times. Representative curves are shown in Figure 2. All three tested inks, mc6, mc8 and mc10, respectively, showed a shear recovery behavior over time. The first low-shear phase displayed higher viscosities of the inks compared to the three following low-shear phases, indicating an initial and not reversible breakage of inner polymer structures after a high shear rate was applied to the pastes. However, the viscosity progress of the pastes at the second, third and fourth low shear region was similar, showing full recovery to the previous state without further significant molecular changes of the polymers after the first high shear rate was applied.

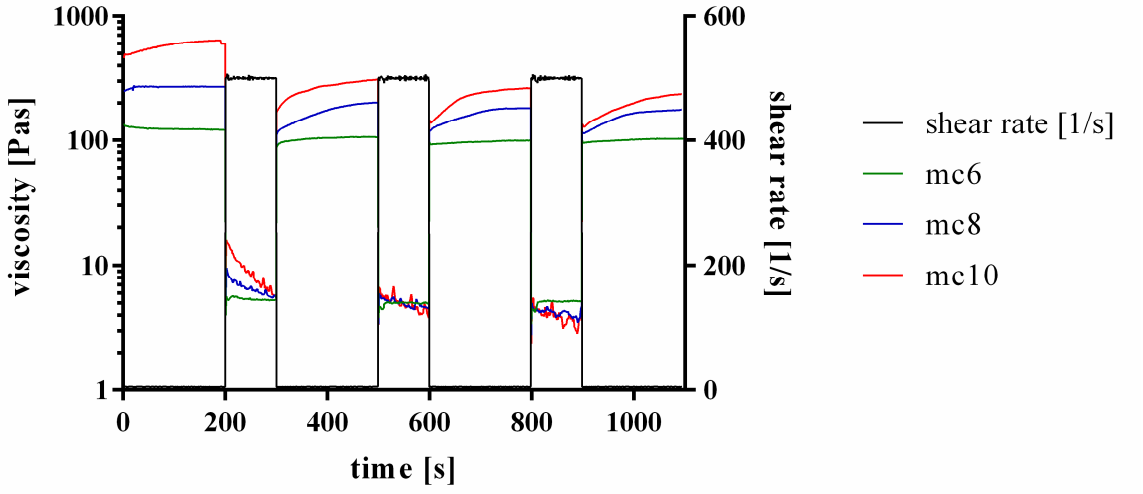

Figure 2. Representative curves of shear recovery experiments of mc6, mc8 and mc10 pastes.

Peer-reviewed version available at Gels 2018, 4, 68; doi:10.3390/gels4030068

2.2 *Extrusion properties of methylcellulose support biomaterial inks*

The extrusion properties were tested using a cylindrical needle with an inner diameter of 250 µm. Firstly, mass flow through the needle was evaluated as function of the applied air pressure (Figure 3). All three pastes showed increased mass flow with increased air pressure, but a significant ($p<0.001$) higher mass flow of the mc6 paste was observed in comparison to mc8 and mc10. For example, at an air pressure of 200 kPa the mass flow of the mc6 paste was 12.72±1.0 mgs^{-1}, whereas the mass flows of mc8 and mc10 were calculated as 0.75±0.12 and 0.19±0.02 mgs^{-1}. Based on these results, the following air pressure values were set for good extrusion with a plotting speed of 10 mms^{-1}: mc6 – 100 kPa, mc8 – 200 kPa and mc10 – 250 kPa.

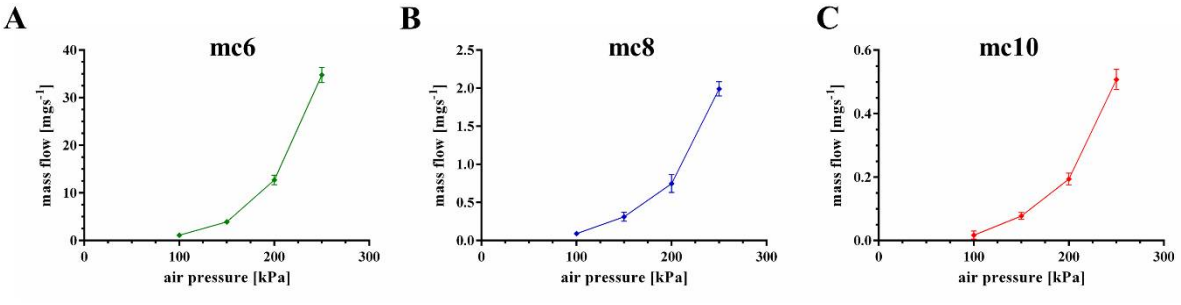

Figure 3. Mass flow of mc6, mc8 and mc10 pastes through a cylindrical needle (inner diameter 250 µm); consider the changes of the y-axes (mean ± SD, n=3).

Shape fidelity of the mc inks was evaluated by filament fusion test, as proposed by Ribeiro and co-workers.[19] Shortly, three layers of the tested ink are plotted on top of each other. The layers are plotted as meanders and the strand distances increase continuously (Figure 4). By comparison of the fused segment length at the meanders to the strand width, the shape fidelity can be evaluated (the quotient should be near to 1.0). The resulting quotients of the filament fusion test are shown in Figure 4 A-C as function of the strand distance. For all pastes the shape fidelity was increased at higher strand distances. In comparison to the mc6 and mc8 biomaterial inks, mc10 displayed the smallest ratios at every strand distance, indicating higher shape fidelity. The measured strand widths of mc6, mc8 and mc10 were 1.20±0.15 mm, 0.75±0.05 mm and 0.62±0.04 mm, respectively; the differences between the strand widths are clearly visible in Figure 4 D-F. This indicates collapses of the inks in z-direction with smallest collapse of the mc10 paste.

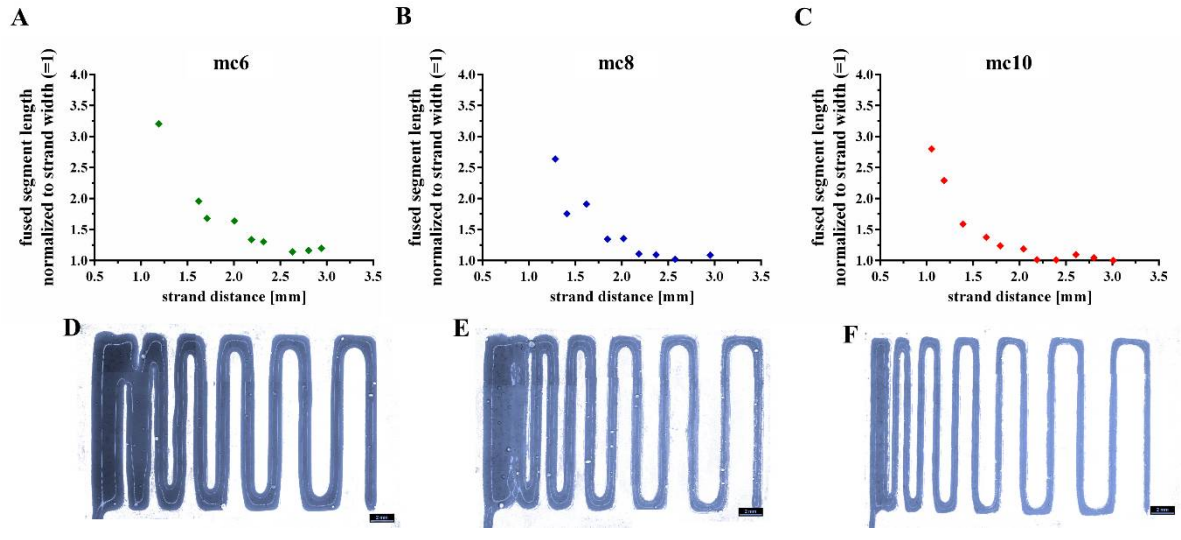

Figure 4. Fused filament test of mc6 (**A,D**), mc8 (**B,E**) and mc10 (**C,F**) pastes.

Based on the results of rheology and extrusion, mc10 was chosen to be the favourit support ink for 3D plotting of complex shaped CPC structures.

2.3 3D plotting of calcium phosphate scaffolds with overhanging structures and inner cavities

Firstly, the shape fidelity of CPC constructs with overhangs was compared to structures of the same geometry, which were plotted without supporting material. The setup of the plotting process is shown in Figure 5 A. A Mayan pyramide with macropores, consisting of CPC was plotted from the large bottom to the small top with a 610 µm needle. The layer structure was clearly visible (Figure 5 B), macropores between the CPC strands were stable after setting and clearly visible in µCT (Figure 5 C). The macroporosity calculated from micro computed tomography data was 69.6 %.

Then, the pyramide was plotted in an inverted orientation displaying critical overhangs which would collapse without supporting material. The principle of plotting is shown in Figure 5 D, by plotting the pyramide from the small top to the large bottom. The turned pyramide was plotted together with the mc10 ink (inner diameter of the needle: 610 µm) as support (Supplementary video SV 1). After plotting and post-processing, methylcellulose could be dried and removed mechanically without alteration of the CPC structure (Figure 5 E). Micro-computed tomography revealed distinct macropores and the determined macroporosity was 66.8 % (Figure 5 F). Whilst the inner structure of the pyramides was comparable to each other without remarkable changes, the boundaries of the pyramides were different. The pyramide plotted without support structure in an upright orientation revealed roundish strands at the borders, while the pyramide plotted with support structure (upside down) had flatten borders and edges, probably as a result of the CPC pressing against the mc at their interface.

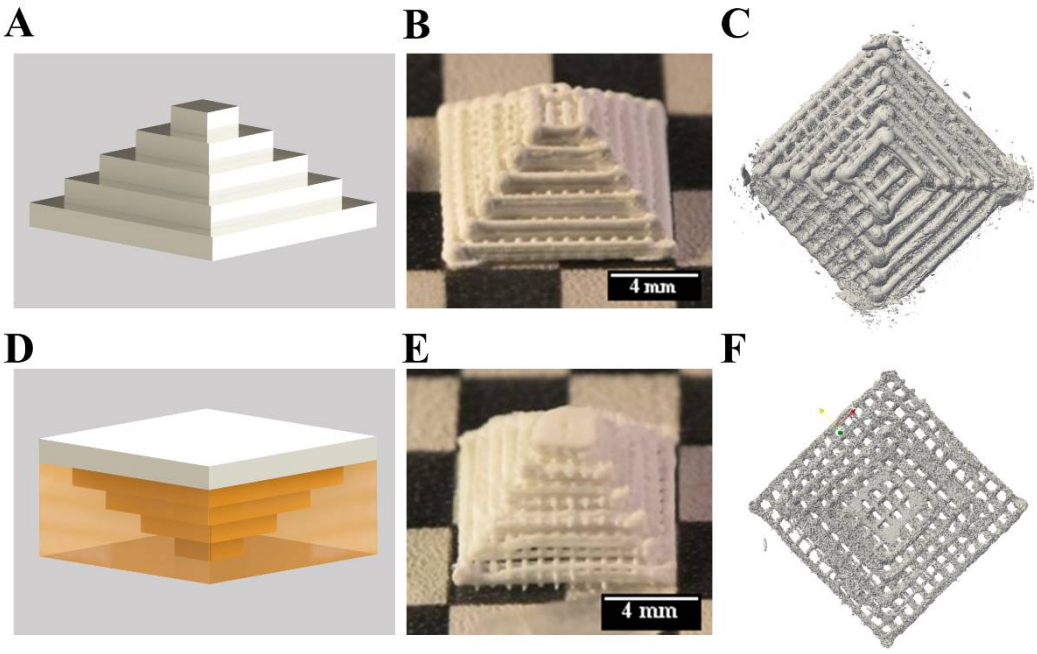

Figure 5. 3D plotting of a Mayan pyramide with and without support structure. Principles (**A**,**D**) show the CPC in white and mc in yellow. The upright and the inverted pyramides (**B**,**C** & **E**,**F**) revealed no changes of the inner structures, but at the borders.

In contrast to a Mayan pyramide, there are structures which cannot be plotted without support. For example, big cavities within a construct would lead to a collapse of the layers plotted above. To demonstrate the suitability of the mc10 support ink for such applications, a cube-inside-cube structure was plotted as shown in Figure 6 A. CPC (strand distance 2 mm) and mc10 were plotted successfully to a cuboid structure of 25x25x25 mm^3. The inner cube plotted with mc10 (plotted without strand distance/macropores) had a volume of 15x15x15 mm^3. After plotting, stereomicroscopical images showed cleary the presence of the unporous mc10 cube (Figure 6 C).

Peer-reviewed version available at Gels 2018, 4, 68; doi:10.3390/gels4030068

Afterwards, the biphasic structure was incubated in humid atmosphere for 3 d, allowing the CPC to set to nanocrystalline HAp. Then, the biphasic scaffold was incubated in distilled water over night at 4 °C. Stereomicroscopy evidenced, that methylcellulose vanished (Figure 6 C) and the pores in z-direction, being closed by mc before, were completely open. Micro-computed tomography and cutting of the CPC structure revealed that the inner cube, which now could be referred to as cavity, preserved the shape of the previous mc cube without collapse of the CPC layers above (Figure 6 D). Additional images demonstrating the achieved even surface of CPC are shown in Supplementary Figure S1.

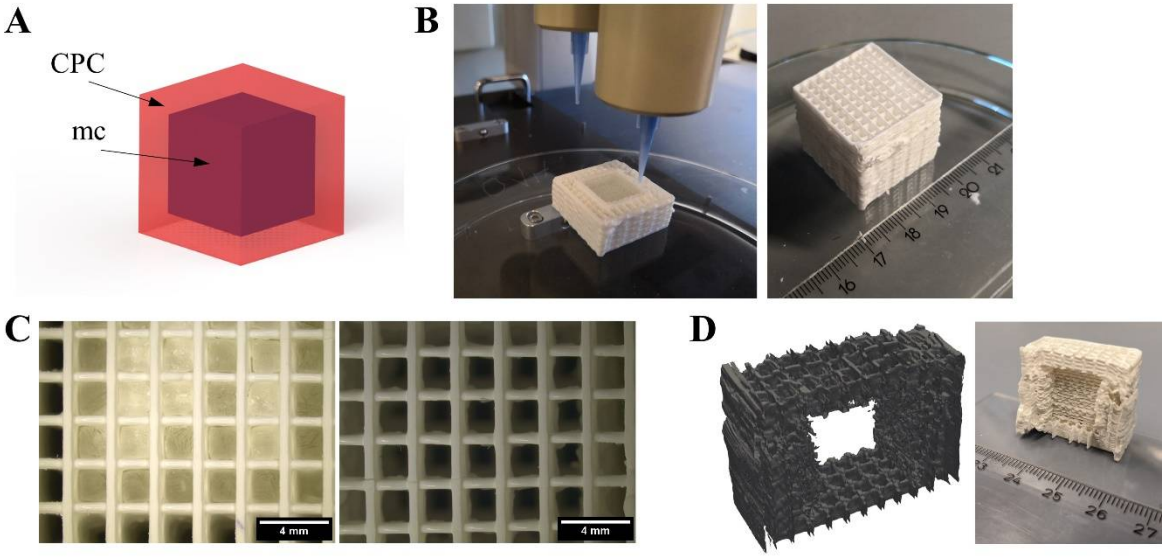

Figure 6. Generation of an inner cavity inside a CPC scaffold. (**A**) Principle of the CPC (red) structure with an inner cavity, filled with support material (mc, purple). (**B**) Fabrication and post-plotting appearance of the cubic structure with 410 µm needles. (**C**) After plotting (left), pores in z-direction of the CPC part are not interconnected but closed by mc at the interface of both materials. After methylcellulose vanished (right), the pores were clearly open and interconnected. (scale bars 4 mm) (**D**) Virtual cut of micro computed tomography of the cube and photograph of the cut cube after mc vanished, revealing the cubical-shaped cavity inside the macroporous CPC structure. More images are provided in Supplementary Figure S1.

2.4 3D plotting of a clinical relevant structure

Plotted CPC structures show great potential for scaffolds in regenerative bone applications. Until now, CPC plotting was already further developed concerning utilization of different material combinations, growth factor loading or integration of live cells into the fabrication process.[20–22] Utilization of methylcellulose as support material opens the window to plot clinical relevant shapes, fitting to patient-specific anatomical structures or individual defects. To show the potential of CPC for these purposes, fabrication of a human scaphoid bone was chosen as example (Figure 7). For this, open source software (Invesalius 3.1 [23]) was used to reconstruct and separate the scaphoid bone from a set of CT data (Figure 7 A). The resulting stl-file was transferred to the BioScaffolder 3.1 software generating the support structure. Afterwards, CPC and mc10 were plotted together layer by layer (Figure 7 B shows CPC in white and mc10 appearing opaque) by usage of needles with an inner diameter of 230 and 250 µm, respectively. Finally, the plotted construct demonstrated high shape equivalence to the stl-file and the characteristic curvature of the anatomical correct scaphoid (Figure 7 C).

Peer-reviewed version available at Gels 2018, 4, 68; doi:10.3390/gels4030068

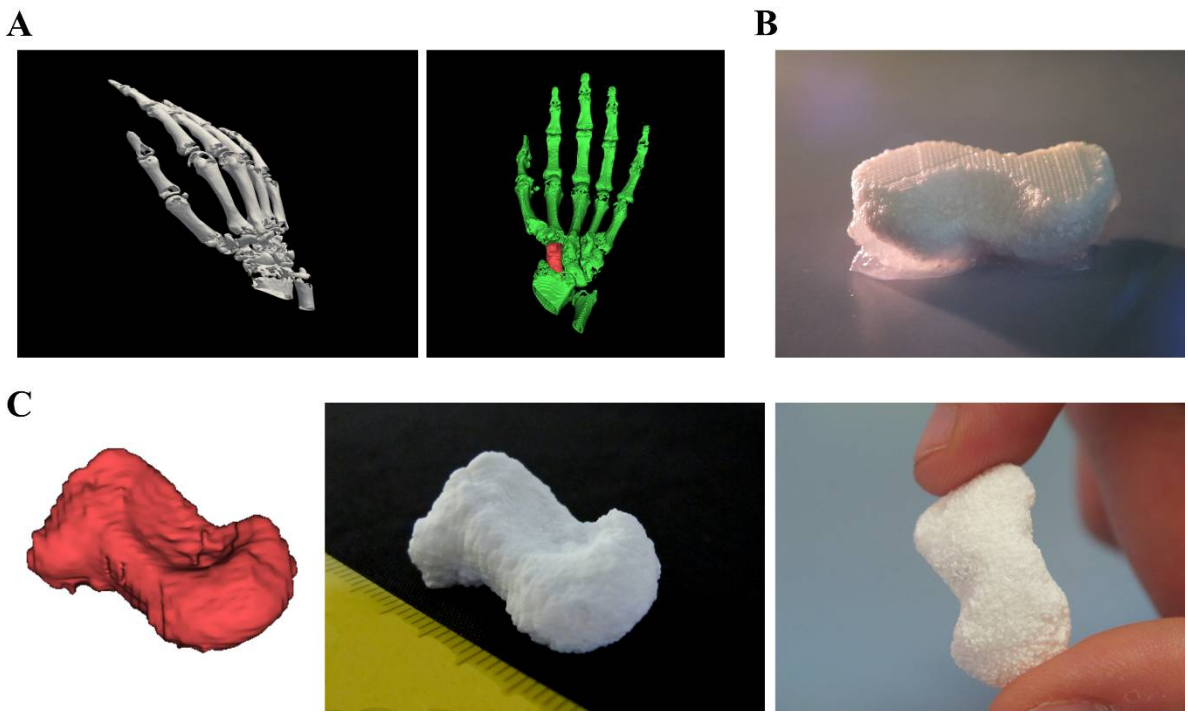

Figure 7. Fabrication of a scaphoid bone from clinical CT data. (**A**) 3D rendered human right hand and selection of the scaphoid by usage of 3D rendering software. (**B**) 3D multichannel plotting of the scaphoid bone consisting of CPC with mc10 as support ink. (**C**) Comparison of the stl-file and the real plotted structure with the characteristic shape of the human scaphoid.

3. Discussion

Methylcellulose was investigated for its use as biomaterial ink for 3D plotting. A concentration of 10 % was convenient to act as support material for plotted structures consisting of a calcium phosphate cement.

Generally, there are two main strategies to apply support to 3D plotted structures: utilization of a supportive bath, which later on gets removed or, as used within this study, the co-extrusion with a temporary support material. For example, the usage of a nanoclay support bath successfully was shown by Jin and co-workers.[24] However, the hydrophilic character of the bath is not applicable for calcium phosphate cements, as the setting reaction would start immediately in the plotting needle, which would result in fast needle clogging. Therefore, an alternative was shown by Miranda and co-workers, who successfully extruded a calcium phosphate cement into a hydrophobic oil-bath, preventing the fast setting reaction and needle clogging.[25] However, the oil bath properties would impair the possibilities of integration of biological sensitive factors and inhibit the inclusion of cells into the plotting process. Thus, co-extrusion of the support is most promising for 3D plotting of complex shaped, anatomical relevant CPC structures. Although the mc10 ink was especially developed for the purpose of support ink for CPC scaffolds, it should be applicable for several other cell-free and cell-laden inks, which act as main structure.

The support ink mostly used for 3D plotting is Pluronic® F127 (poloxamer 407 – a synthetic, nonionic triblock copolymer). Previous studies investigated its use to create channel-like structures or sacrificial molds.[26–28] Herein, we successfully have developed a support ink based on methylcellulose, specifically applicable for a self-setting CPC. Methylcellulose has comparable thermoresponsive properties like Pluronic® F127 (so it can be easily dissolved at 4 °C within a few hours), but additionally was shown to be released out of an alginate matrix over time at 37 °C.[29] In

Peer-reviewed version available at Gels 2018, 4, 68; doi:10.3390/gels4030068

a recent study of our group, we have observed, that mc dissolution at 37 °C is ongoing over 21 days, which can be influenced by control of the molecular weight.[30] This might be advantageous for future applications, as the vanishing of the support ink does not necessarily have to occur at one time point. Moreover, the utilization of mc as new support material opens up new fabrication methods; for example, some inks are based on Pluronic® F127,[31] and might need another material as sacrificial support structure which can be dissolved at temperatures at which Pluronic® F127 is stable.

The plotting properties of the tested mc support inks were strongly dependent on their concentration. Especially mc10 and mc8 showed a good printability and furthermore shape fidelity after extrusion, whereas plotted mc6 strands tended to collapse. The enhancement of shape fidelity of materials for 3D plotting was shown before in blends with alginate or a nanoclay-alginate composite.[29,32]. Pure cellulose, or derivatives like bacterial nanocellulose were used to enhance viscosity and shape fidelity of 3D plotted scaffolds and cell-laden constructs.[33–35] However, the adjustable solubility of mc makes it an optimal material as support ink, which can vanish at a defined time point.

Herein, we have proven the suitability of co-plotting mc as support material for CPC constructs. Rheological and extrusion properties were investigated, showing high applicability for extrusion-based additive manufacturing. The viscosity of mc was increasing with increasing concentration. However, further development of mc-based support inks could involve the presence of additives in the support paste. The gel point, and thus the gel strength/viscosity of mc can be adjusted by additives like sucrose, propylene glycol or glycerin, which should impact the dissolution properties.[36] Recently, it was shown, that cationic dodecyltrimethylammonium salts (bromide, DTAB) was lowering the gel strength of mc;[37] as the gel point of mc was strongly depressed, this principle could help to further control the dissolution process of plotted mc support structures.

For the first time, CPC was plotted with a support ink to obtain complex shaped constructs of clinical relevance. In the past, complex shaped calcium phosphate scaffolds were manufactured by powder printing,[38–40] or selective laser sintering[41] with the powder bed automatically also working as stabilizing support. Calcium phosphate scaffolds, fabricated by stereolithography, did not collapse, due to the stabilizing effect of the surrounding resin, before the resulting scaffolds were sintered.[42,43] Furthermore, calcium phosphate scaffolds were additively manufactured by indirect printing [44], lithography-based ceramic manufacturing [45] or robocasting [25]. All of these methods have in common, that combination with biologically sensitive proteins is difficult and the inclusion of cells into the fabrication process is impossible. In contrast, extrusion of CPC is conducted in mild conditions (at room or physiological temperature, without any organic solvents involved or energy-intensive post-processing steps etc.). This enables fabrication of CPC together with temperature sensitive substances even living cells.[16,21,46] Therefore, 3D plotting of CPC with support material does not only allow creation of complex shaped structures or implants, but also enables biofunctionalization of calcium phosphate implants in a spatially defined manner, which is superior to most other additive manufacturing methods.

Firstly, the influence of plotting a support structure together with a CPC main structure was evaluated. The inner structure of the tested pyramids was not affected, whereas the outer borders were changed distinctly. The pyramid plotted without support comprised more roundish strands, as it is expected for strands at a surface of every plotted scaffold. In contrast, the pyramid plotted with mc10 as support ink in reversed orientation revealed flattened strands at the interface to mc. Both, roundish and flattened strands are approximations of the real geometry of the pyramid. In case of a possible implant there are neither right angles nor complete convex surfaces. Therefore, the geometry of a single strand might never mimic the real geometry of a human bone specimen. As the resorption of the nanocrystalline HAp by osteoclasts is part of the natural bone remodeling process,[47,48] the surface of plotted CPC implants will change over the whole healing time; thus, the strand surface does not necessarily have to reproduce the real surface of the bone completely. However, the rough

geometry of anatomical structures can be plotted: the example of the human scaphoid bone showed sufficient shape reproduction in comparison with the three-dimensional image file. Parameters influencing the plotted shape were on the one hand the resolution of the computed tomography data set and the precision of the generation of the stl-file. On the other hand, the strand distance and orientation, the used needle diameters for extrusion of CPC and mc and plotting properties like the layer thickness, applied air pressure and plotting velocity influence the outcome significantly. For CPC, these parameters were optimized in our group, achieving filigree strands and scaffolds with high inner complexity.[46]

Crucially, CPC scaffolds could be fabricated containing large inner cavities. Such closed inner pores can only by generated by additive manufacturing methods. The dissolution properties of mc allowed fast vanishing of the internal mc cube after CPC was set (3 days), leaving behind a cavity of the desired cubic shape. This might enable the fabrication of scaffolds with highly controlled (macro)porosity to improve the ingrowth of cells and vascular structures, both accepted as main challenges in bone tissue engineering.

4. Conclusion

The usage of a newly developed methylcellulose-based support ink was sufficient to enable fabrication of structures with critical overhangs and to produce controlled cavities inside a CPC construct. For the first time it was shown that CPC can be used to fabricate constructs of any clinical and anatomical relevant shape by 3D plotting. Furthermore, a human scaphoid bone model of high shape-fidelity could be produced. Further work should concentrate on more control of the dissolution properties of mc, which basically could be tailored for any application by addition of gel-strengthening and gel-weakening substances. The principle of biphasic plotting of the support ink and CPC will facilitate the production of patient-individual HAp implants, fabricated by 3D plotting.

5. Materials and Methods

5.1 Preparation of plotting paste

CPC was manufactured by InnoTERE GmbH (Radebeul, Germany). For the support material, methylcellulose powder (M0512, Sigma, USA, molecular weight ≈88 kDa, 4000 cP) was dissolved for 12 h in deionized water at 4 °C in different concentrations (6 w/v %, 8 w/v % and 10 w/v, respectively). To ensure full binding of water to mc, solutions were stirred every 2 h. The resulting support inks are referred to as mc6, mc8 and mc10.

5.2 Rheology

Rheological examinations of the mc pastes were performed with a plate-plate rheometer (Rheotest RN 4, Medingen, Germany; d = 36 mm, distance of the plates 0.1 mm). Shear thinning was characterized by increasing the shear rate from 0-100 s^{-1} over 1200 s (increment 0.08 s^{-1}) and viscosity was measured (n=3). Shear recovery of the mc pastes was characterized orientating at the protocols proposed by Paxton and co-workers and Kesti and co-workers [17,18]. Firstly, a constant shear rate of 5 s^{-1} was applied for 200 s, followed by a hundred-fold higher shear rate of 500 s^{-1} for 100 s. This procedure was repeated two times. Then, again a shear rate of 5 s^{-1} was applied for 200 s. For the whole time of observation, viscosity was measured and shear recovery was obtained.

5.3 Mass flow and filament fusion test

The mass flow of mc6, mc8 and mc10 was conducted through a conical needle with an inner diameter of 250 µm (Globaco, Rödermark, Germany). The inks were allowed to flow through the needle for 50 s at different air pressures (100, 150, 200, 250 kPa), then the mass of the extruded volume was measured. Resulting mass flow $\dot{m}$ was calculated:

Peer-reviewed version available at Gels 2018, 4, 68; doi:10.3390/gels4030068

$$\dot{m} = \frac{m}{50\ s}$$

Filament fusion tests of the mc inks were performed following the protocol of Ribeiro and co-workers.[19] Shortly, three layers of the inks were plotted on top of each other. Each layer consisted of meandering strands with increasing strand distances. Immediately after plotting, the scaffolds were imaged by a stereo light microscope (Leica M205 C equipped with DFC295 camera, Germany). Resulting images were analyzed by Fiji Image software [49] and actual strand distance, fused segment length and strand width were obtained from the data. The quotient of segment length to strand width was evaluated as function of the strand distance.

5.4 Fabrication of volumetric constructs and post-fabrication treatment

Both, CPC and mc support inks, were filled into cartridges and plotted to scaffolds (sizes given in Figure captions) utilizing a three-axis multichannel plotter (BioScaffolder 3.1, GeSiM mbH, Radeberg, Germany). The needle (Globaco) dependent plotting parameters are summarized in Table 1. After plotting, CPC was allowed to set in water-saturated atmosphere (>95 %) for 3 d. Afterwards, residual mc of biphasic CPC-mc constructs was dissolved in water at 4 °C.

Table 1. Plotting parameters of CPC and mc support inks

Material ink	Needle size [µm]	Air pressure [kPa]	Printing speed [mms^{-1}]	Layer thickness [µm]
CPC	230	250	10	120
	410	200	10	260
	610	150	10	360
mc6	250	100	10	120
mc8	250	200	10	120
mc10	250	250	10	120
	410	180	10	260
	610	130	10	360

5.5 Microcomputed tomography

Micro X-ray computed tomography was conducted by a custom-built setup called TomoTU of TU Dresden, Institute of Fluid Mechanics, Chair of Magnetofluiddynamics, Measurement and Automation Technology. The grey value images of the sample were generated with 0.5° angular increment (720 images in total) for a tube current of 170 µA and an acceleration voltage of 90 kV. The size of the photodiode array and therefore of the images was 2304 x 2940 (vertical x horizontal) pixel. A magnification of 3.55 was chosen, which resulted in a resolution of 1 pixel = 13.95 µm. Reconstructions of the 3D-images was created by grey value analysis (threshold = 120) with Paraview 5.5 software.[50] Macroporosity of the scaffolds was determined by grey value analysis of the reconstructed image stacks (threshold = 120).

Author Contributions: Conceptualization T.A., A.L. and M.G., Experimental, data analysis and visualization T.A., T.K. and C.C.; Funding attraction A.L., M.G.; Supervision A.L., M.G.; Paper writing and editing T.A., C.C., A.L., M.G.

Funding: This research was funded by the German Federal Ministry for Economic Affairs and Energy (BMWi) in collaboration with the German Federation of Industrial Research Associations (AiF; ZIM project, contract No. KF3359301AK4) and by the European Social Fund (ESF) together with the Free State of Saxony in course of the Young Researchers Group "IndivImp".

Acknowledgments: The authors thank Ms. Ortrud Zieschang and MSc Anna-Maria Placht for excellent technical assistance and Dr. Stefan Günther and Prof. Stefan Odenbach for support at the TomoTU and fruitful discussion about results of micro-computed tomography.

Conflicts of Interest: The authors declare no conflicts of interest.

References

1. Probst, F. A.; Hutmacher, D. W.; Müller, D. F.; Machens, H.-G.; Schantz, J.-T. Calvarial reconstruction by customized bioactive implant. *Handchir Mikrochir Plast Chir* **2010**, *42*, 369–373, doi:10.1055/s-0030-1248310.
2. Melchels, F.; Wiggenhauser, P. S.; Warne, D.; Barry, M.; Ong, F. R.; Chong, W. S.; Hutmacher, D. W.; Schantz, J.-T. CAD/CAM-assisted breast reconstruction. *Biofabrication* **2011**, *3*, 034114, doi:10.1088/1758-5082/3/3/034114.
3. Landers, R.; Pfister, A.; Hübner, U.; John, H.; Schmelzeisen, R.; Mülhaupt, R. Fabrication of soft tissue engineering scaffolds by means of rapid prototyping techniques. *J Mater Sci* **2002**, *37*, 3107–3116, doi:10.1023/A:1016189724389.
4. Mir, T. A.; Nakamura, M. Three-Dimensional Bioprinting: Toward the Era of Manufacturing Human Organs as Spare Parts for Healthcare and Medicine. *Tissue Engineering Part B: Reviews* **2017**, *23*, 245–256, doi:10.1089/ten.teb.2016.0398.
5. Kilian, D.; Ahlfeld, T.; Akkineni, A. R.; Lode, A.; Gelinsky, M. Three-dimensional bioprinting of volumetric tissues and organs. *MRS Bulletin* **2017**, *42*, 585–592, doi:10.1557/mrs.2017.164.
6. Malda, J.; Visser, J.; Melchels, F. P.; Jüngst, T.; Hennink, W. E.; Dhert, W. J. A.; Groll, J.; Hutmacher, D. W. 25th Anniversary Article: Engineering Hydrogels for Biofabrication. *Adv. Mater.* **2013**, *25*, 5011–5028, doi:10.1002/adma.201302042.
7. Sanz, T.; Fernández, M. A.; Salvador, A.; Muñoz, J.; Fiszman, S. M. Thermogelation properties of methylcellulose (MC) and their effect on a batter formula. *Food Hydrocoll* **2005**, *19*, 141–147, doi:10.1016/j.foodhyd.2004.04.023.
8. Nasatto, P. L.; Pignon, F.; Silveira, J. L. M.; Duarte, M. E. R.; Noseda, M. D.; Rinaudo, M. Methylcellulose, a Cellulose Derivative with Original Physical Properties and Extended Applications. *Polymers* **2015**, *7*, 777–803, doi:10.3390/polym7050777.
9. Swan, K. C. USE OF METHYL CELLULOSE IN OPHTHALMOLOGY. *Arch Ophthalmol* **1945**, *33*, 378–380, doi:10.1001/archopht.1945.00890170054004.
10. Inactive Ingredient Search for Approved Drug Products Available online: https://www.accessdata.fda.gov/scripts/cder/iig/index.cfm (accessed on Jul 9, 2018).
11. Maazouz, Y.; B. Montufar, E.; Guillem-Marti, J.; Fleps, I.; Öhman, C.; Persson, C.; P. Ginebra, M. Robocasting of biomimetic hydroxyapatite scaffolds using self-setting inks. *J Mater Chem B* **2014**, *2*, 5378–5386, doi:10.1039/C4TB00438H.
12. Maazouz, Y.; Montufar, E. B.; Malbert, J.; Espanol, M.; Ginebra, M.-P. Self-hardening and thermoresponsive alpha tricalcium phosphate/pluronic pastes. *Acta Biomater* **2017**, *49*, 563–574, doi:10.1016/j.actbio.2016.11.043.
13. Heinemann, S.; Rössler, S.; Lemm, M.; Ruhnow, M.; Nies, B. Properties of injectable ready-to-use calcium phosphate cement based on water-immiscible liquid. *Acta Biomater* **2013**, *9*, 6199–6207, doi:10.1016/j.actbio.2012.12.017.

Peer-reviewed version available at Gels 2018, 4, 68; doi:10.3390/gels4030068

14. Lode, A.; Meissner, K.; Luo, Y.; Sonntag, F.; Glorius, S.; Nies, B.; Vater, C.; Despang, F.; Hanke, T.; Gelinsky, M. Fabrication of porous scaffolds by three-dimensional plotting of a pasty calcium phosphate bone cement under mild conditions. *J Tissue Eng Regen Med* **2014**, *8*, 682–693, doi:10.1002/term.1563.
15. Barba, A.; Diez-Escudero, A.; Maazouz, Y.; Rappe, K.; Espanol, M.; Montufar, E. B.; Bonany, M.; Sadowska, J. M.; Guillem-Marti, J.; Öhman-Mägi, C.; Persson, C.; Manzanares, M.-C.; Franch, J.; Ginebra, M.-P. Osteoinduction by foamed and 3D-printed calcium phosphate scaffolds: effect of nanostructure and pore architecture. *ACS Appl. Mater. Interfaces* **2017**, doi:10.1021/acsami.7b14175.
16. Akkineni, A. R.; Luo, Y.; Schumacher, M.; Nies, B.; Lode, A.; Gelinsky, M. 3D plotting of growth factor loaded calcium phosphate cement scaffolds. *Acta Biomater* **2015**, *27*, 264–274, doi:10.1016/j.actbio.2015.08.036.
17. Paxton, N.; Smolan, W.; Böck, T.; Melchels, F.; Groll, J.; Jungst, T. Proposal to assess printability of bioinks for extrusion-based bioprinting and evaluation of rheological properties governing bioprintability. *Biofabrication* **2017**, *9*, 044107, doi:10.1088/1758-5090/aa8dd8.
18. Kesti, M.; Fisch, P.; Pensalfini, M.; Mazza, E.; Zenobi-Wong, M. Guidelines for standardization of bioprinting: a systematic study of process parameters and their effect on bioprinted structures. *BioNanoMaterials* **2016**, *17*, 193–204, doi:10.1515/bnm-2016-0004.
19. Ribeiro, A.; Blokzijl, M. M.; Levato, R.; Visser, C. W.; Castilho, M.; Hennink, W. E.; Vermonden, T.; Malda, J. Assessing bioink shape fidelity to aid material development in 3D bioprinting. *Biofabrication* **2018**, *10*, 014102, doi:10.1088/1758-5090/aa90e2.
20. Akkineni, A. R.; Ahlfeld, T.; Lode, A.; Gelinsky, M. A versatile method for combining different biopolymers in a core/shell fashion by 3D plotting to achieve mechanically robust constructs. *Biofabrication* **2016**, *8*, 045001, doi:10.1088/1758-5090/8/4/045001.
21. Luo, Y.; Lode, A.; Sonntag, F.; Nies, B.; Gelinsky, M. Well-ordered biphasic calcium phosphate–alginate scaffolds fabricated by multi-channel 3D plotting under mild conditions. *J. Mater. Chem. B* **2013**, *1*, 4088–4098, doi:10.1039/C3TB20511H.
22. Ahlfeld, T.; Doberenz, F.; Kilian, D.; Vater, C.; Korn, P.; Lauer, G.; Lode, A.; Gelinsky, M. Bioprinting of mineralized constructs utilizing multichannel plotting of a self-setting calcium phosphate cement and a cell-laden bioink. *Biofabrication* **2018**, doi:10.1088/1758-5090/aad36d.
23. Amorim, P.; Moraes, T.; Silva, J.; Pedrini, H. InVesalius: An Interactive Rendering Framework for Health Care Support. In *Advances in Visual Computing*; Springer, Cham, 2015; pp. 45–54.
24. Jin, Y.; Liu, C.; Chai, W.; Compaan, A.; Huang, Y. Self-Supporting Nanoclay as Internal Scaffold Material for Direct Printing of Soft Hydrogel Composite Structures in Air. *ACS Appl. Mater. Interfaces* **2017**, *9*, 17456–17465, doi:10.1021/acsami.7b03613.
25. Miranda, P.; Saiz, E.; Gryn, K.; Tomsia, A. P. Sintering and robocasting of β-tricalcium phosphate scaffolds for orthopaedic applications. *Acta Biomater* **2006**, *2*, 457–466, doi:10.1016/j.actbio.2006.02.004.

26. Müller, M.; Becher, J.; Schnabelrauch, M.; Zenobi-Wong, M. Printing Thermoresponsive Reverse Molds for the Creation of Patterned Two-component Hydrogels for 3D Cell Culture. *J Vis Exp* **2013**, doi:10.3791/50632.
27. Kolesky, D. B.; Truby, R. L.; Gladman, A. S.; Busbee, T. A.; Homan, K. A.; Lewis, J. A. 3D Bioprinting of Vascularized, Heterogeneous Cell-Laden Tissue Constructs. *Adv Mater 26*, 3124–3130, doi:10.1002/adma.201305506.
28. Suntornnond, R.; Tan, E. Y. S.; An, J.; Chua, C. K. A highly printable and biocompatible hydrogel composite for direct printing of soft and perfusable vasculature-like structures. *Sci Rep* **2017**, *7*, 16902, doi:10.1038/s41598-017-17198-0.
29. Schütz, K.; Placht, A.-M.; Paul, B.; Brüggemeier, S.; Gelinsky, M.; Lode, A. Three-dimensional plotting of a cell-laden alginate/methylcellulose blend: towards biofabrication of tissue engineering constructs with clinically relevant dimensions. *J Tissue Eng Regen Med* **2017**, *11*, doi:10.1002/term.2058.
30. Hodder, E.; Duin, S.; Kilian, D.; Ahlfeld, T.; Seidel, J.; Nachtigall, C.; Bush, P.; Covill, D.; Gelinsky, M.; Lode, A. Investigating the effect of sterilisation methods on the physical properties and cytocompatibility of methyl cellulose used in combination with alginate for 3D-bioplotting of chondrocytes. *J Mater Sci Mater Med* (under review).
31. Gioffredi, E.; Boffito, M.; Calzone, S.; Giannitelli, S. M.; Rainer, A.; Trombetta, M.; Mozetic, P.; Chiono, V. Pluronic F127 Hydrogel Characterization and Biofabrication in Cellularized Constructs for Tissue Engineering Applications. *Procedia CIRP* **2016**, *49*, 125–132, doi:10.1016/j.procir.2015.11.001.
32. Ahlfeld, T.; Cidonio, G.; Kilian, D.; Duin, S.; Akkineni, A. R.; Dawson, J. I.; Yang, S.; Lode, A.; Oreffo, R. O. C.; Gelinsky, M. Development of a clay based bioink for 3D cell printing for skeletal application. *Biofabrication* **2017**, *9*, 034103, doi:10.1088/1758-5090/aa7e96.
33. Li, L.; Zhu, Y.; Yang, J. 3D bioprinting of cellulose with controlled porous structures from NMMO. *Materials Lett* **2018**, *210*, 136–138, doi:10.1016/j.matlet.2017.09.015.
34. Markstedt, K.; Mantas, A.; Tournier, I.; Martínez Ávila, H.; Hägg, D.; Gatenholm, P. 3D Bioprinting Human Chondrocytes with Nanocellulose-Alginate Bioink for Cartilage Tissue Engineering Applications. *Biomacromolecules* **2015**, *16*, 1489–1496, doi:10.1021/acs.biomac.5b00188.
35. Wang, Q.; Sun, J.; Yao, Q.; Ji, C.; Liu, J.; Zhu, Q. 3D printing with cellulose materials. *Cellulose* **2018**, 1–27, doi:10.1007/s10570-018-1888-y.
36. Levy, G.; Schwarz, T. W. The Effect Of Certain Additives On The Gel Point Of Methylcellulose**University of California School of Pharmacy, San Francisco 22. *J Am Pharm Assoc* **1958**, *47*, 44–46, doi:10.1002/jps.3030470113.
37. Villetti, M. A.; Bica, C. I. D.; Garcia, I. T. S.; Pereira, F. V.; Ziembowicz, F. I.; Kloster, C. L.; Giacomelli, C. Physicochemical Properties of Methylcellulose and Dodecyltrimethylammonium Bromide in Aqueous Medium. *J Phys Chem B* **2011**, *115*, 5868–5876, doi:10.1021/jp110247r.
38. Castilho, M.; Moseke, C.; Ewald, A.; Gbureck, U.; Groll, J.; Pires, I.; Teßmar, J.; Elke Vorndran Direct 3D powder printing of biphasic calcium phosphate scaffolds for

substitution of complex bone defects. *Biofabrication* **2014**, *6*, 015006, doi:10.1088/1758-5082/6/1/015006.

39. Seitz, H.; Deisinger, U.; Leukers, B.; Detsch, R.; Ziegler, G. Different Calcium Phosphate Granules for 3-D Printing of Bone Tissue Engineering Scaffolds. *Adv Eng Mater 11*, B41–B46, doi:10.1002/adem.200800334.
40. Vorndran, E.; Klarner, M.; Klammert, U.; Grover, L. M.; Patel, S.; Barralet, J. E.; Gbureck, U. 3D Powder Printing of β-Tricalcium Phosphate Ceramics Using Different Strategies. *Advanced Engineering Materials 10*, B67–B71, doi:10.1002/adem.200800179.
41. Duan, B.; Wang, M.; Zhou, W. Y.; Cheung, W. L.; Li, Z. Y.; Lu, W. W. Three-dimensional nanocomposite scaffolds fabricated via selective laser sintering for bone tissue engineering. *Acta Biomater* **2010**, *6*, 4495–4505, doi:10.1016/j.actbio.2010.06.024.
42. Bian, W.; Li, D.; Lian, Q.; Li, X.; Zhang, W.; Wang, K.; Jin, Z. Fabrication of a bio‐inspired beta‐Tricalcium phosphate/collagen scaffold based on ceramic stereolithography and gel casting for osteochondral tissue engineering. *Rapid Prototyp J* **2012**, *18*, 68–80, doi:10.1108/13552541211193511.
43. Seol, Y.-J.; Kim, J. Y.; Park, E. K.; Kim, S.-Y.; Cho, D.-W. Fabrication of a hydroxyapatite scaffold for bone tissue regeneration using microstereolithography and molding technology. *Microelectron Eng* **2009**, *86*, 1443–1446, doi:10.1016/j.mee.2009.01.053.
44. Schumacher, M.; Deisinger, U.; Detsch, R.; Ziegler, G. Indirect rapid prototyping of biphasic calcium phosphate scaffolds as bone substitutes: influence of phase composition, macroporosity and pore geometry on mechanical properties. *J Mater Sci: Mater Med* **2010**, *21*, 3119–3127, doi:10.1007/s10856-010-4166-6.
45. Pfaffinger, M.; Hartmann, M.; Schwentenwein, M.; Stampfl, J. Stabilization of tricalcium phosphate slurries against sedimentation for stereolithographic additive manufacturing and influence on the final mechanical properties. *Int J Appl Ceram Tec 14*, 499–506, doi:10.1111/ijac.12664.
46. Ahlfeld, T.; Akkineni, A. R.; Förster, Y.; Köhler, T.; Knaack, S.; Gelinsky, M.; Lode, A. Design and Fabrication of Complex Scaffolds for Bone Defect Healing: Combined 3D Plotting of a Calcium Phosphate Cement and a Growth Factor-Loaded Hydrogel. *Ann Biomed Eng* **2017**, *45*, 224–236, doi:10.1007/s10439-016-1685-4.
47. Bernhardt, A.; Schumacher, M.; Gelinsky, M. Formation of Osteoclasts on Calcium Phosphate Bone Cements and Polystyrene Depends on Monocyte Isolation Conditions. *Tissue Eng Part C Methods* **2014**, *21*, 160–170, doi:10.1089/ten.tec.2014.0187.
48. Kular, J.; Tickner, J.; Chim, S. M.; Xu, J. An overview of the regulation of bone remodelling at the cellular level. *Clin Biochem* **2012**, *45*, 863–873, doi:10.1016/j.clinbiochem.2012.03.021.
49. Schindelin, J.; Arganda-Carreras, I.; Frise, E.; Kaynig, V.; Longair, M.; Pietzsch, T.; Preibisch, S.; Rueden, C.; Saalfeld, S.; Schmid, B.; Tinevez, J.-Y.; White, D. J.; Hartenstein, V.; Eliceiri, K.; Tomancak, P.; Cardona, A. Fiji: an open-source platform for biological-image analysis. *Nat Methods* **2012**, *9*, 676–682, doi:10.1038/nmeth.2019.

50. Ahrens, J.; Geveci, B.; Law, C. ParaView: An End-User Tool for Large-Data Visualization. In *Visualization Handbook*; Elsevier, 2005; pp. 717–731 ISBN 978-0-12-387582-2.